nature geoscience

ARTICLES

https://doi.org/10.1038/s41561-019-0456-x

Australian hot and dry extremes induced by weakenings of the stratospheric polar vortex

Eun-Pa Lim[1*], Harry H. Hendon[1], Ghyslaine Boschat[2,3], Debra Hudson[1], David W. J. Thompson[4], Andrew J. Dowdy[1] and Julie M. Arblaster[2,3,5]

The occurrence of extreme hot and dry conditions in warm seasons can have large impacts on human health, energy and water supplies, agriculture and wildfires. Australian hot and dry extremes have been known to be associated with the occurrence of El Niño and other variations of tropospheric circulation. Here we identify an additional driver: variability of the stratospheric Antarctic polar vortex. On the basis of statistical analyses using observational data covering the past 40 yr, we show that weakenings and warmings of the stratospheric polar vortex, which episodically occur during austral spring, substantially increase the chances of hot and dry extremes and of associated fire-conducive weather across subtropical eastern Australia from austral spring to early summer. The promotion of these Australian climate extremes results from the downward coupling of the weakened polar vortex to tropospheric levels, where it is linked to the low-index polarity of the Southern Annular Mode, an equatorward shift of the mid-latitude westerly jet stream and subsidence and warming in the subtropics. Because of the long timescale of the polar vortex variations, the enhanced likelihood of early-summertime hot and dry extremes and wildfire risks across eastern Australia may be predictable a season in advance during years of vortex weakenings.

Understanding, predicting and anticipating extreme high temperature and low rainfall in the warm seasons is crucially important in Australia because of the risks and impacts on human health, agriculture, wildfires, utilities, infrastructure and water management[1]. In particular, the impact of the reduced productivity of dairy and meat under extreme hot and dry conditions can be felt beyond Australia as Australia is one of the world's major exporters of these products[2]. The warm phase of the El Niño–Southern Oscillation (ENSO)[3], the positive phase of the Indian Ocean Dipole (IOD)[4] and the negative index polarity of the Southern Annular Mode (SAM)[5] are important drivers of extreme hot and dry conditions over various regions of Australia, mainly in spring but to some extent in summer as well[6–8]. Here we highlight that a weaker than normal springtime stratospheric polar vortex over Antarctica is a key driver and an important source of predictability of extreme hot and dry climate conditions over subtropical eastern Australia during its warm seasons. Anomalous weakening of the Southern Hemisphere polar stratospheric vortex in spring is shown to subsequently promote the negative polarity of the SAM, which then promotes Australian high daytime temperature and low rainfall extremes and associated dangerous atmospheric conditions for wildfire from mid-spring to early summer.

The stratospheric polar vortex, which occurs in both hemispheres, is characterized by maximum westerly winds in the upper stratosphere–lower mesosphere that circle the hemisphere. It is strongest in the winter half of the year and disappears during summer, making its seasonal progression from the mid-latitudes towards the pole from early winter to spring[9–11]. This seasonal march also involves a downward progression of the maximum westerlies from the upper stratosphere in winter to the lower troposphere in spring which is caused by vigorous interactions with planetary-scale waves travelling upward from the troposphere that act to decelerate the westerly vortex. The polar vortex in the Northern Hemisphere (NH) is mainly perturbed during boreal winter to early spring[11,12], and the Southern Hemisphere (SH) vortex is perturbed during austral winter to spring[13,14]. Variability of the stratospheric polar vortex produced by variability of upward-propagating planetary-scale waves can couple downward to the troposphere and promote low-frequency variations in tropospheric circulation and temperature, thus serving as a source of extended-range predictability of surface weather and climate[15–18]. For example, downward coupling from the stratosphere to the troposphere in association with sudden stratospheric warmings in the NH, which commonly occurs in boreal winter and early spring, often results in sustained impacts on surface climate via promoting the negative polarity of the North Atlantic Oscillation/Northern Annular Mode[15,19,20].

Although generally not as spectacular as sudden stratospheric warming events in the NH, stratospheric polar vortex variations episodically occur in the SH in austral spring to early summer[21,22]. Anomalous SH stratospheric polar vortex weakening or intensification during spring, which can be viewed as an earlier or later shift in the seasonal evolution of the vortex, respectively[17,23], can lead to sustained occurrence of the negative or positive polarity of the tropospheric SAM (in this study, SAM denotes tropospheric SAM unless otherwise stated), respectively, during spring–summer[15,17,18,24,25]. The SAM is well recognized to drive variations in surface climate throughout the SH, including changes in precipitation and surface temperatures[6,26–28], via the concomitant latitudinal shifts in the extratropical storm track and edge of the Hadley circulation[29,30]. Impacts of the SAM on Australian climate are particularly pronounced, causing changes in extreme maximum and minimum temperatures and rainfall across much of the southern and eastern parts of the continent, especially during spring and summer[6,7,27,31].

[1]Bureau of Meteorology, Melbourne, Victoria, Australia. [2]ARC Centre of Excellence for Climate Extremes, Monash University, Clayton, Victoria, Australia. [3]School of Earth, Atmosphere and Environment, Monash University, Clayton, Victoria, Australia. [4]Department of Atmospheric Science, Colorado State University, Fort Collins, CO, USA. [5]National Center for Atmospheric Research, Boulder, CO, USA. *e-mail: e.lim@bom.gov.au

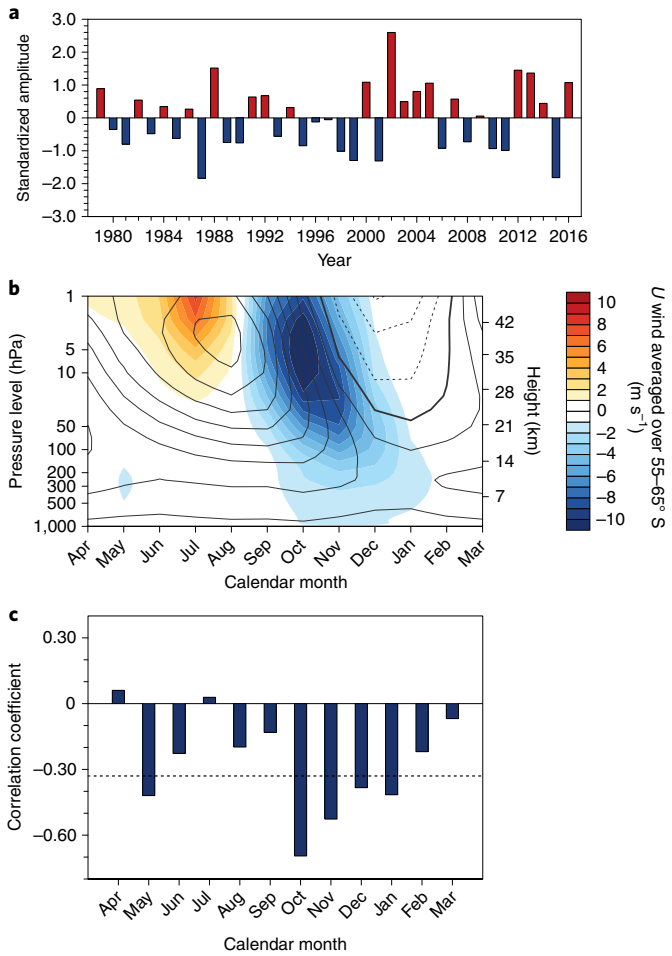

Fig. 1 | The S–T coupled mode and its relationship with the SAM. **a**,**b**, The S–T coupled mode index (**a**) and its eigenvector (**b**), which represent the interannual variability of the SH stratospheric polar vortex and its downward coupling[18]. The positive phase of the S–T coupled mode represents weakening of the SH spring polar vortex. In **b**, the S–T coupled mode eigenvector (colour shading) is overlaid by the climatological zonal-mean zonal wind (*U* wind) averaged over 55–65° S (contours). Negative contours indicating easterlies are dashed, and the zero contour is thickened. The contour interval is 10 m s^{-1}. **c**, Correlation between the S–T coupled mode index and monthly SAM (CPC AAO)[18]. The horizontal dashed line indicates the correlation statistically significant at the 5% level, assessed by a two-tailed Student *t* test with 38 samples.

Identifying the years of SH polar vortex weakening

This study builds on Lim et al.[18], who objectively identified years when the SH stratospheric polar vortex significantly weakened and broke down earlier than normal during spring, with the resultant weakened westerly winds propagating downward from the stratosphere to the surface during spring to early summer (Fig. 1a,b, Methods and Supplementary Fig. 1). The opposite can also happen, with a late breakdown of the vortex driving anomalously strong westerly winds. Lim et al. demonstrated a strong connection of this stratosphere–troposphere (S–T) coupling to the subsequent variation of the SAM during October–January (Fig. 1c), which drives the variation of surface climate throughout the SH[18].

Here we select the nine years when the Antarctic polar vortex was most significantly weaker than normal in spring during the period of 1979–2016, as judged by the amplitude of the S–T coupled mode index[18] equal to or greater than 0.8 standard deviation (σ) (Fig. 1a and Methods). The nine years 1979, 1988, 2000, 2002, 2004, 2005, 2012, 2013 and 2016 have been identified as significant vortex weakening years, most of which are also marked by significantly earlier final breakdown dates of the SH stratospheric polar vortex (Supplementary Fig. 1). We then examine the subsequent variation of October–January mean Australian daily maximum temperature (T_{max}), daily minimum temperature (T_{min}), rainfall and wildfire potential as measured by the McArthur Forest Fire Danger Index (FFDI)[32]. We also monitor variations in the SAM, mean sea-level pressure (MSLP), geopotential height and vertical velocity at the 500 hPa level (GPH500 and ω500, respectively) and total cloud cover. We compare the means of these variables in the 9 significant vortex weakening years to the control group of the other 29 yr when the S–T coupled mode index had weak positive or negative amplitudes (that is, when the S–T coupled mode index $<0.8\sigma$). We include the years of SH stratospheric vortex strengthening in the control group because their impact on Australian climate is not much different from the normal conditions (Methods). To focus on the impact of the SH polar vortex variation that is independent of ENSO, we removed the influence of ENSO from the variables examined here using linear regression (Methods). We also detrended all data for the period 1979–2016 to concentrate on the impacts of year-to-year variations of the polar vortex.

Impact of vortex weakening on Australian seasonal climate

The composite difference of T_{max}, T_{min} and rainfall anomalies averaged over October–January for the significant nine polar vortex weakening years (vortex weakening years) compared with the control group of all the other years (vortex non-weakening years) is displayed in Fig. 2. During the vortex weakening years, the strongest positive T_{max} anomalies occurred over subtropical eastern Australia—Queensland, New South Wales and northeastern South Australia (130–156° E, 10–30° S; see Supplementary Fig. 2 for the locations of Australian states and territory)—where the 4-month mean anomaly is significantly higher, reaching up to 2 °C. Coincident rainfall reduction is found over most of eastern Australia but especially over central Queensland. The significant increases of T_{max} and decreases of rainfall during the vortex weakening years are statistically robust at the 5% level, assessed by a permutation resampling test[33] (two-sided) using 4,000 random resamples (Methods). However, T_{min} appears to be relatively less sensitive to polar vortex weakening; therefore, we exclude T_{min} in the subsequent analysis and discussion.

Occurrences of extreme seasonal mean T_{max} and rainfall are especially affected by significant vortex weakening. We compute the ratio of the probability of occurrence of extreme events during the vortex weakening years to that during the vortex non-weakening years using two definitions of an extreme event. In the first case, we examine the occurrence of a top-quintile hottest year (that is, top 20%, which equates to the 7 hottest events in the 38-yr record) and a bottom-quintile driest year using the October–January mean T_{max} and rainfall, respectively (Fig. 3a,b). Consistent with the mean anomalies during the vortex weakening years, the probability of a year being in the top quintile for T_{max} and bottom quintile for rainfall increases up to four to eight times for large regions of Queensland and northern New South Wales. The blue-shaded region in Fig. 3a (labelled as x/0, where x represents the probability of occurrence of an extreme event during the vortex weakening years) indicates that T_{max} being in the top quintile only ever occurred during vortex weakening years in the study period of 1979–2016.

As extreme high temperature and low rainfall are favourable conditions for wildfires[32], the probability of occurrence of dangerous fire-weather conditions being in the top quintile (as indicated by the FFDI; Methods) also significantly increases four to eight times during the vortex weakening years over almost all of Queensland, northern New South Wales and northeastern South Australia (Fig. 3c). The far west region of Western Australia is also vulnerable to increased wildfire danger during the vortex weakening years.

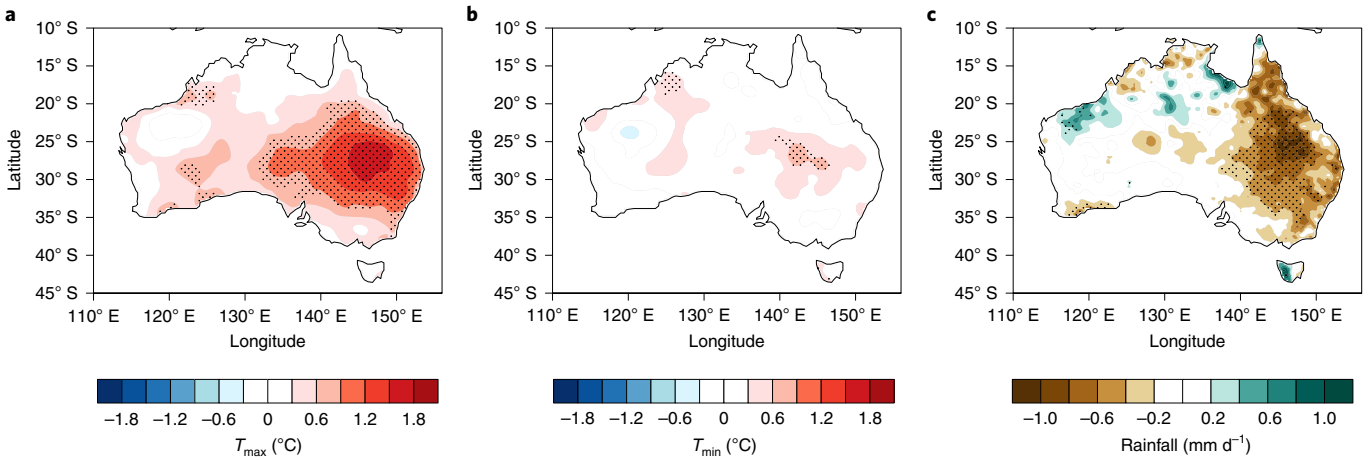

Fig. 2 | Anomalous Australian climate conditions during the nine polar vortex weakening years. a–c, Composite difference of October–January mean daily maximum temperature (T_{max}) (**a**), daily minimum temperature (T_{min}) (**b**) and rainfall (**c**) during the 9 significant stratospheric polar vortex weakening years compared to the 29 vortex non-weakening years. The contour interval is 0.3 °C for T_{max} and T_{min} and 0.2 mm d^{-1} for rainfall. Stippling indicates statistically significant difference at the 5% level, assessed by a permutation test (two-sided) with 4,000 times of random resampling without replacement. Influence of ENSO and the linear trends over the period 1979–2016 were removed from the data before the composite calculation.

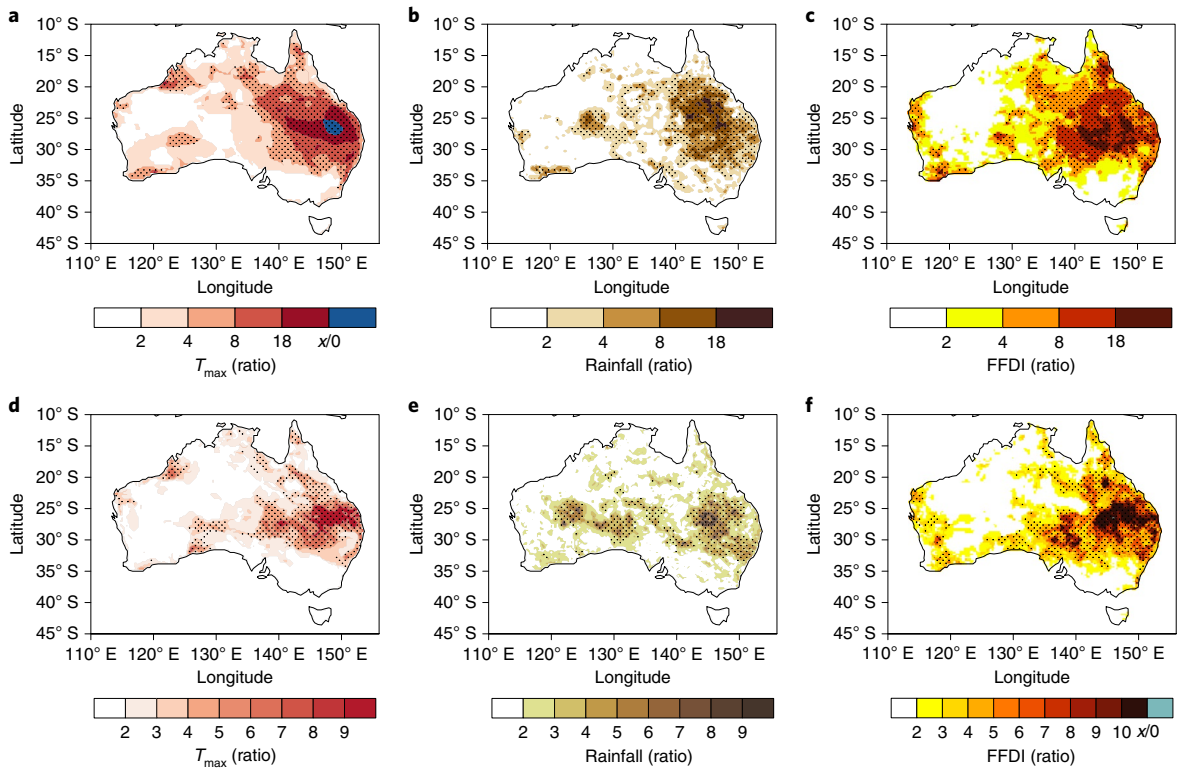

Fig. 3 | Changes in the likelihood of extreme high T_{max}, low rainfall and high wildfire danger during the nine polar vortex weakening years. a, Ratio of the probability of occurrence of top-quintile October–January mean T_{max} during the 9 significant vortex weakening years to that during the 29 vortex non-weakening years. **b**,**c**, Same as **a** except bottom-quintile rainfall (**b**) and top-quintile FFDI (**c**). **d**–**f**, Same as **a**–**c**, respectively, except top-decile monthly T_{max} (**d**), bottom-decile monthly rainfall (**e**) and top-decile monthly FFDI (**f**) during October–January. The blue colour shading in **a** and **f** (labelled *x*/0 on the colour bar) indicates that the top 20% T_{max} events (the 7 hottest events in 1979–2016) and the top 10% wildfire danger (the 15 highest-danger periods among 152 months of October–January in the 38 yr) occurred only during the significant vortex weakening years (one grid box at 26.5° S and 146° E falls into this case in **f**). Stippling indicates statistical significance at the 2.5% level, assessed by a permutation test (one-sided) with the null hypothesis that the ratio of the probability of occurrence of an extreme event during the vortex weakening years to all other years is 1.

We also look at the occurrence of individual months during October–January for having T_{max} and rainfall in the top and bottom deciles (10%), respectively (Fig. 3d,e). Similar to Fig. 3a,b, there is a greater than four times increase in the probability of occurrence of monthly mean T_{max} being in the top decile and monthly mean rainfall being in the bottom decile over southern Queensland during the

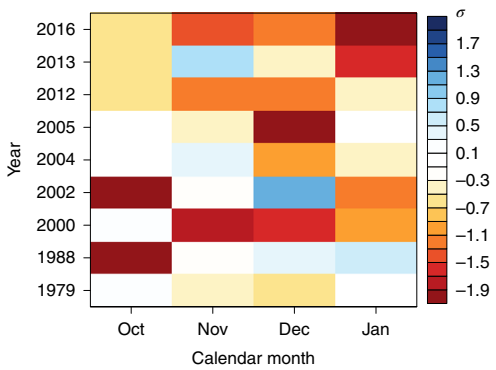

Fig. 4 | Monthly standardized SAM index anomalies during the nine polar vortex weakening years. The mean value of the standardized SAM index for these nine years during October–January is −0.7. The SAM index used is independent of ENSO and its 38-yr long-term trend as described in Methods. The years labelled on the vertical axis indicate the years of October–December when vortex weakening occurred in the SH polar stratosphere.

vortex weakening years. Consequently, the chance for a month during October to January having dangerous fire-weather conditions substantially increases over southern Queensland and northeastern South Australia during the vortex weakening years (Fig. 3f). These increases in the frequency of extreme hot and dry events and associated wildfire danger in October–January following the weakening and early breakdown of the stratospheric polar vortex in spring are statistically significant at the 2.5% level, assessed by a one-sided permutation test (Methods).

We have repeated these calculations without first removing the trend and the linear relationship with ENSO. We find that the probability of occurrence of October to January mean extreme high T_{max}, low rainfall and high fire-weather risks still increases by up to a factor of four in the same areas of eastern Australia during the vortex weakening years (Supplementary Fig. 3). The probability of extreme monthly T_{max} and related fire danger also still increases by greater than four times during the vortex weakening years while the probability of the extreme low monthly rainfall increases by two to three times. These results highlight the role of stratospheric polar vortex weakening for driving extreme hot, dry and fire-prone atmospheric conditions in subtropical eastern Australia during spring–summer.

How the SH polar vortex is linked to Australian climate

Weakening of the Antarctic polar vortex during spring promotes the negative polarity of the SAM (Fig. 1c), whose anomalous hemispheric pressure pattern is characterized by zonally symmetric low-pressure anomalies in the mid-latitudes and high-pressure anomalies in the high latitudes[5,18]. Figure 4 shows that the SAM tends to be persistently negative during October–January when the polar vortex weakens and breaks down early. This persistence is an important characteristic of the negative polarity of the SAM driven by the stratospheric vortex weakening, which appears to amplify the impact of the SAM on extreme climate conditions over Australia. The negative polarity of the SAM that is not coupled to the stratospheric polar vortex weakening is less persistent through the warm season (Supplementary Fig. 4) and appears to have less impact on extreme climate conditions (Supplementary Fig. 5) than the negative SAM that is coupled to the stratospheric polar vortex weakening (Fig. 3).

The negative polarity of the SAM is associated with lower-than-normal surface pressure over Australia and stronger-than-normal surface westerlies to the south of Australia[6]. The pattern of surface pressure and wind differences during October–January in vortex weakening years is consistent with this typical negative polarity SAM pattern (Fig. 5a). However, the difference in surface winds between the vortex weakening years and non-weakening years is not statistically significant over subtropical eastern Australia.

In contrast to the lower-than-normal surface pressure, mid-tropospheric geopotential height over Australia is significantly more positive during vortex weakening years (Fig. 5b), and there is increased downward motion, indicated by positive anomalies of ω500 (Fig. 5c). Total cloud cover is also substantially reduced over eastern Australia during the vortex weakening years (Fig. 5d). The increased downward motion and reduced cloud cover over Australia reflect an equatorward shift of the edge of the downward branch of the SH Hadley cell in the austral warm seasons, which has previously been shown to be a dynamical response to the negative polarity of the SAM[29,30,34]. The locations of reduced cloud cover and enhanced subsidence are coincident with the regions of enhanced T_{max} and reduced rainfall over eastern Australia (see also Supplementary Figs. 6–10). Together, these anomalies support the notion that positive temperature anomalies in the eastern part of Australia are primarily promoted by anomalous adiabatic warming due to enhanced subsidence and increased insolation associated with reduced cloud cover[35]. Reduced rainfall also contributes to higher temperature as less soil moisture is available for evaporative cooling. The significant increases of mid-tropospheric geopotential height and downward motion imply that the negative surface pressure anomalies over Australia associated with the negative polarity of the SAM during the vortex weakening years are likely to be thermally driven with a shallow vertical structure. Warm and dry northwesterlies associated with the low-pressure centre south of Australia could bring hot and dry air to the east and contribute to the extreme hot and dry climate in eastern Australia, as observed in 2005 and 2016 (Supplementary Fig. 11).

Prospect for skilful prediction of SH extreme climate

We have highlighted the connection of anomalous weakening of the SH stratospheric polar vortex with significantly enhanced occurrences of extreme hot and dry conditions over eastern Australia during the warm seasons. Persistent negative polarity of the SAM is promoted by the stratospheric polar vortex weakening, which induces anomalous sinking of air and a clearer sky over eastern Australia and appears to serve as a pathway for the stratospheric polar vortex signal to affect subtropical eastern Australian climate conditions. Previous studies have demonstrated predictability of the SAM during spring and summer arising from its connection to ENSO[36–38], but the current results suggest that SAM variability induced by stratospheric variations during October to January is independent of ENSO and has greater impact on subtropical eastern Australian climate than does ENSO. Lim et al.[18] reported that S–T coupling during the spring months is often preconditioned by anomalies in upward-propagating planetary wave activity and a meridional shift of the vortex as high as the stratopause and as early as June. Thus, we might anticipate increased chances of occurrence of extreme hot and dry conditions in late spring to early summer at least a season in advance when the Antarctic stratospheric polar vortex shows an anomalous signal as early as winter[17,18].

Previous work[24] has reported that the springtime Antarctic polar vortex variability and associated tropospheric SAM variation can be skilfully predicted in a dynamical seasonal climate forecast system when initialized at the beginning of August. This capability implies the potential for long-lead predictive skill for the occurrence of not only Australian extreme climate but also extreme climate in other regions of the SH that are affected by the SAM variation, including Antarctic sea ice[18,28,39] in the spring and summer seasons. This predictability arising from variations of the polar stratosphere would be in addition to predictability arising from ENSO, which is traditionally viewed as the main source of long-lead predictability for global

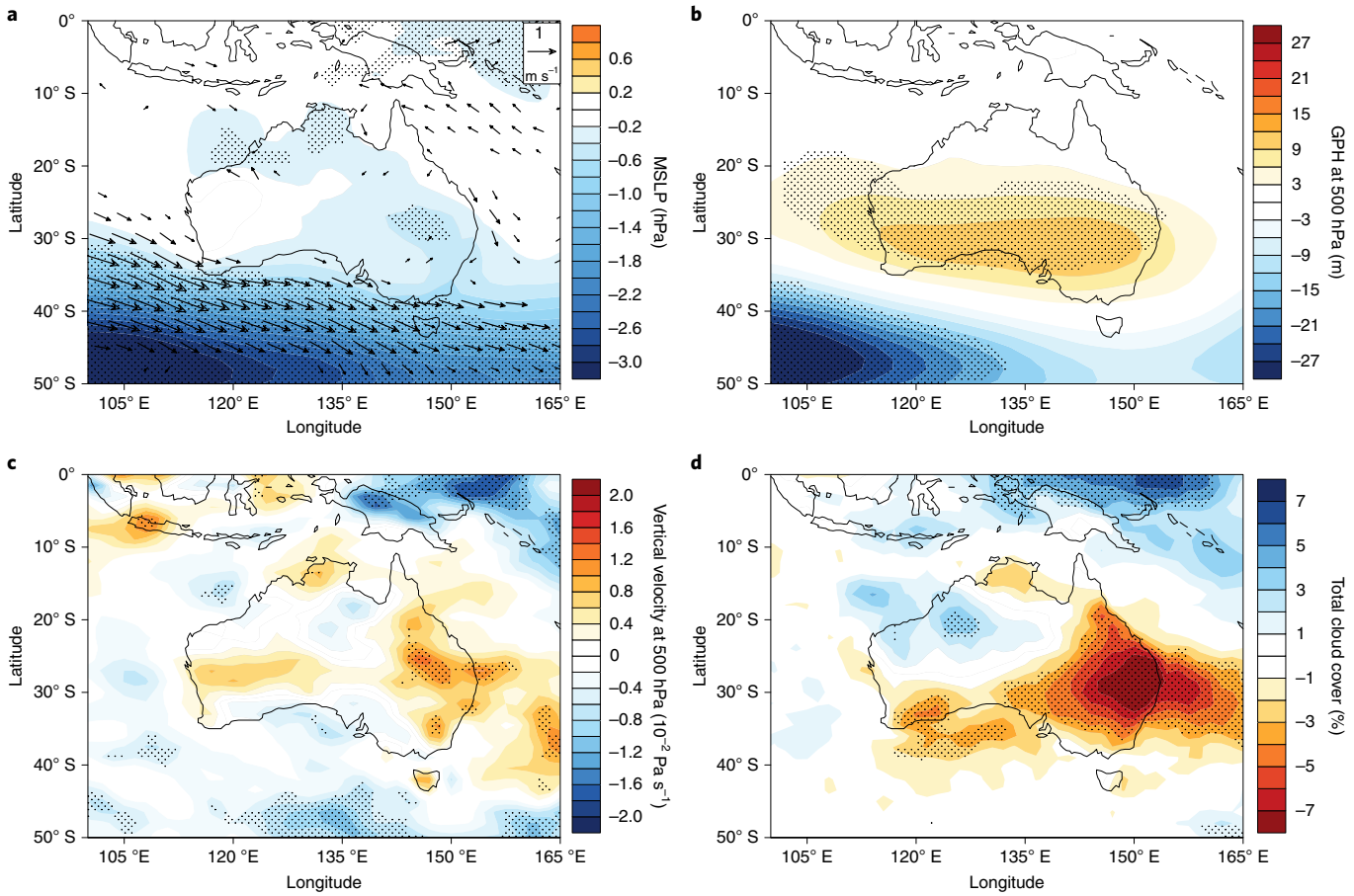

Fig. 5 | Circulation and cloud cover changes over Australia during the nine polar vortex weakening years. a–d, Composite difference of October–January mean MSLP (**a**), GPH500 (**b**), ω500 (**c**) and total cloud cover anomalies (**d**) during the 9 vortex weakening years compared to the 29 vortex non-weakening years. The contour interval is 0.2 hPa, 3 m, 0.002 Pa s^{-1} and 0.01 (as fraction) for MSLP, GPH500, ω500 and total cloud cover, respectively. Stippling indicates statistically significant difference at the 10% level, assessed by a permutation test (two-sided).

climate. Future research efforts will focus on exploring predictability of extreme climate conditions provided by polar stratospheric variations using the Australian Bureau of Meteorology's new sub-seasonal to seasonal climate forecast system, ACCESS-S1[40], which well resolves the stratosphere but runs with prescribed climatological ozone. Ozone in the lower stratospheric polar vortex inversely varies with the strength of the vortex, and because ozone efficiently absorbs incoming ultraviolet radiation, ozone variations can act to anomalously warm or cool the vortex, thereby acting to extend the impact of the vortex variation to surface climate during summer[28,41,42]. Implementation of prognostic ozone may be a key area for development of improved climate prediction systems, especially in light of the expected recovery of the Antarctic ozone hole in coming decades[43].

Online content

Any methods, additional references, Nature Research reporting summaries, source data, statements of code and data availability and associated accession codes are available at https://doi.org/10.1038/s41561-019-0456-x.

Received: 24 April 2019; Accepted: 28 August 2019;
Published online: 07 October 2019

References

1. Managing Climate Variability R&D Program. *Climate Kelpie* http://managingclimate.gov.au/publications/improved-seasonal-forecasts-the-benefits-for-agriculture-other-sectors-and-australias-economy/
2. Australian Government Department of Agriculture Meat, wool and dairy. *Australian Government* http://www.agriculture.gov.au/ag-farm-food/meat-wool-dairy (2019).
3. Bjerknes, J. Atmospheric teleconnections from the equatorial Pacific. *Mon. Weather Rev.* **97**, 163–172 (1959).
4. Saji, N. H., Goswami, B. N., Vinayachandran, P. N. & Yamagata, T. A dipole mode in the tropical Indian Ocean. *Nature* **401**, 360–363 (1999).
5. Thompson, D. W. J. & Wallace, J. M. Annular mode in the extratropical circulation. Part I: month-to-month variability. *J. Clim.* **13**, 1000–1016 (2000).
6. Hendon, H. H., Thompson, D. W. J. & Wheeler, M. C. Australian rainfall and surface temperature variations associated with the Southern Hemisphere annular mode. *J. Clim.* **20**, 2452–2467 (2007).
7. Min, S.-K., Cai, W. & Whetton, P. Influence of climate variability on seasonal extremes over Australia. *J. Geophys. Res. Atmos.* **118**, 643–654 (2013).
8. Perkins, S. E., Argüeso, D. & White, C. J. Relationships between climate variability, soil moisture, and Australian heatwaves. *J. Geophys. Res. Atmos.* **120**, 8144–8164 (2015).
9. Hirota, I., Hirooka, T. & Shiotani, M. Upper stratospheric circulations in the two hemispheres observed by satellites. *Q. J. R. Meteorol. Soc.* **109**, 443–454 (1983).
10. Kodera, K. & Kuroda, Y. Dynamical response to the solar cycle. *J. Geophys. Res. Atmos.* **107**, 4749 (2002).
11. Waugh, D. W., Sobel, A. H. & Polvani, L. M. What is the polar vortex and how does it influence weather? *Bull. Am. Meteorol. Soc.* **98**, 37–44 (2017).
12. McIntyre, M. E. How well do we understand the dynamics of stratospheric warmings? *J. Meteorol. Soc. Jpn Ser. II* **60**, 37–65 (1982).
13. Randel, W. J. The seasonal evolution of planetary-waves in the Southern Hemisphere stratosphere and troposphere. *Q. J. R. Meteorol. Soc.* **114**, 1385–1409 (1988).
14. Hio, Y. & Yoden, S. Interannual variations of the seasonal march in the Southern Hemisphere stratosphere for 1979–2002 and characterization of the unprecedented year 2002. *J. Atmos. Sci.* **62**, 567–580 (2005).

15. Baldwin, M. P. et al. Stratospheric memory and skill of extended-range weather forecasts. *Science* **301**, 636–640 (2003).
16. Charlton, A. J., O'Neill, A., Stephenson, D. B., Lahoz, W. A. & Baldwin, M. P. Can knowledge of the state of the stratosphere be used to improve statistical forecasts of the troposphere? *Q. J. R. Meteorol. Soc.* **129**, 3205–3224 (2003).
17. Byrne, N. J. & Shepherd, T. G. Seasonal persistence of circulation anomalies in the Southern Hemisphere stratosphere and its implications for the troposphere. *J. Clim.* **31**, 3467–3483 (2018).
18. Lim, E.-P., Hendon, H. H. & Thompson, D. W. J. Seasonal evolution of stratosphere–troposphere coupling in the Southern Hemisphere and implications for the predictability of surface climate. *J. Geophys. Res. Atmos.* **123**, 12002–12016 (2018).
19. Sigmond, M., Scinocca, J. F., Kharin, V. V. & Shepherd, T. G. Enhanced seasonal forecast skill following stratospheric sudden warmings. *Nat. Geosci.* **6**, 98–102 (2013).
20. Baldwin, M. P. & Dunkerton, T. J. Propagation of the Arctic Oscillation from the stratosphere to the troposphere. *J. Geophys. Res. Atmos.* **104**, 30937–30946 (1999).
21. Shiotani, M. & Hirota, I. Planetary wave-mean flow interaction in the stratosphere: a comparison between Northern and Southern hemispheres. *Q. J. R. Meteorol. Soc.* **111**, 309–334 (1985).
22. Kuroda, Y. & Kodera, K. Interannual variability in the troposphere and stratosphere of the Southern Hemisphere winter. *J. Geophys. Res. Atmos.* **103**, 13787–13799 (1998).
23. Shiotani, M., Shimoda, N. & Hirota, I. Interannual variability of the stratospheric circulation in the Southern Hemisphere. *Q. J. R. Meteorol. Soc.* **119**, 531–546 (1993).
24. Seviour, W. J. M. et al. Skillful seasonal prediction of the Southern Annular Mode and Antarctic ozone. *J. Clim.* **27**, 7462–7474 (2014).
25. Thompson, D. W. J., Baldwin, M. P. & Solomon, S. Stratosphere–troposphere coupling in the Southern Hemisphere. *J. Atmos. Sci.* **62**, 708–715 (2005).
26. Thompson, D. W. J. & Solomon, S. Interpretation of recent Southern Hemisphere climate change. *Science* **296**, 895–899 (2002).
27. Gillett, N. P., Kell, T. D. & Jones, P. D. Regional climate impacts of the Southern Annular Mode. *Geophys. Res. Lett.* **33**, L23704 (2006).
28. Bandoro, J., Solomon, S., Donohoe, A., Thompson, D. W. J. & Santer, B. D. Influences of the Antarctic ozone hole on southern hemispheric summer climate change. *J. Clim.* **27**, 6245–6264 (2014).
29. Kang, S. M., Polvani, L. M., Fyfe, J. C. & Sigmond, M. Impact of polar ozone depletion on subtropical precipitation. *Science* **332**, 951–954 (2011).
30. Hendon, H. H., Lim, E.-P. & Nguyen, H. Seasonal variations of subtropical precipitation associated with the Southern Annular Mode. *J. Clim.* **27**, 3446–3460 (2014).
31. Lim, E. P. & Hendon, H. H. Understanding the contrast of Australian springtime rainfall of 1997 and 2002 in the frame of two flavors of El Niño. *J. Clim.* **28**, 2804–2822 (2015).
32. Dowdy, A. J. Climatological variability of fire weather in Australia. *J. Appl. Meteorol. Climatol.* **57**, 221–234 (2018).
33. Wilks, D. S. *Statistical Methods in the Atmospheric Sciences* (Academic Press, 2006).
34. Ceppi, P. & Hartmann, D. L. On the speed of the eddy-driven jet and the width of the Hadley cell in the Southern Hemisphere. *J. Clim.* **26**, 3450–3465 (2013).
35. Quinting, J. F., Parker, T. J. & Reeder, M. J. Two synoptic routes to subtropical heat waves as illustrated in the Brisbane region of Australia. *Geophys. Res. Lett.* **45**, 10700–10708 (2018).
36. L'Heureux, M. L. & Thompson, D. W. J. Observed relationships between the El Niño–Southern Oscillation and the extratropical zonal-mean circulation. *J. Clim.* **19**, 276–287 (2006).
37. Zhou, T. J. & Yu, R. C. Sea-surface temperature induced variability of the Southern Annular Mode in an atmospheric general circulation model. *Geophys. Res. Lett.* **31**, L24206 (2004).
38. Lim, E.-P., Hendon, H. H. & Rashid, H. Seasonal predictability of the Southern Annular Mode due to its association with ENSO. *J. Clim.* **26**, 8037–8054 (2013).
39. Wang, G. et al. Compounding tropical and stratospheric forcing of the record low Antarctic sea-ice in 2016. *Nat. Commun.* **10**, 13 (2019).
40. Hudson, D. A. et al. ACCESS-S1: the new Bureau of Meteorology multi-week to seasonal prediction system. *J. South. Hemisph. Earth Syst. Sci.* **67**, 132–159 (2017).
41. Shaw, T. A., Perlwitz, J., Harnik, N., Newman, P. A. & Pawson, S. The impact of stratospheric ozone changes on downward wave coupling in the Southern Hemisphere. *J. Clim.* **24**, 4210–4229 (2011).
42. Gillett, Z. E. et al. Evaluating the relationship between interannual variations in the Antarctic ozone hole and Southern Hemisphere surface climate in chemistry–climate models. *J. Clim.* **32**, 3131–3151 (2019).
43. Solomon, S. et al. Emergence of healing in the Antarctic ozone layer. *Science* **353**, 269–274 (2016).

Acknowledgements

This study is part of the Forewarned is Forearmed project, which is supported by funding from the Australian Government Department of Agriculture as part of its Rural R&D for Profit programme. G.B. and J.M.A. were supported by the Australian Research Council Centre of Excellence for Climate Extremes (grant CE170100023). J.M.A. was also supported by the Regional and Global Model Analysis component of the Earth and Environmental System Modeling Program of the US Department of Energy's Office of Biological & Environmental Research via National Science Foundation IA 1947282. A.J.D. was supported by funding from the Australian Government's National Environmental Science Program. D.W.J.T. was supported by the NSF Climate and Large-Scale Dynamics Program. We thank T. Cowan and B. Trewin at the Bureau of Meteorology for their constructive feedback on the manuscript. We also thank M. Griffiths at the Bureau of Meteorology for processing AWAP data for the analysis of the study. This research was undertaken at the NCI National Facility in Canberra, Australia, which is supported by the Australian Commonwealth Government. The NCAR Command Language (NCL; http://www.ncl.ucar.edu) version 6.4.0 was used for data analysis and visualization of the results. We also acknowledge NCAR/UCAR, NOAA, ECMWF and the Japanese Met Agent for producing and providing the Hurrell et al. (2008) SST analysis, the Reynolds OI v2 SST analysis, the ERA-Interim reanalysis and the JRA-55 reanalysis, respectively.

Author contributions

E.-P.L. and H.H.H. conceived ideas for the study, E.-P.L. and G.B. conducted data analysis, H.H.H. wrote the first version of the manuscript and all authors contributed to the interpretation of the results and the writing of the manuscript.

Competing interests

The authors declare no competing interests.

Additional information

Supplementary information is available for this paper at https://doi.org/10.1038/s41561-019-0456-x.

Correspondence and requests for materials should be addressed to E.-P.L.

Peer review information Primary Handling Editor(s): Heike Langenberg.

Reprints and permissions information is available at www.nature.com/reprints.

Publisher's note Springer Nature remains neutral with regard to jurisdictional claims in published maps and institutional affiliations.

Methods

Datasets. We used MSLP, GPH500, ω500 and total cloud cover from the ERA-Interim (ECMWF re-analysis-Interim) reanalysis[44]. Monthly mean fields are available on 1.5° horizontal grids. Variations of Australian temperatures and rainfall are explored using the gridded analyses from the Australian Water Availability Project (AWAP)[45], which are available on a 5 km grid beginning in 1900 for rainfall and 1910 for temperatures. The AWAP analyses are from an optimum interpolation of the available station observations across Australia. Daily maximum and minimum temperatures and rainfall are available, for which we computed monthly means. For compatibility with the available ERA-Interim data, we restricted our analyses to the period 1979–2017.

Climate indices. The S–T coupled mode pattern and index were obtained following Lim et al.[18] by applying height–time domain empirical orthogonal function (EOF) analysis to anomalies (seasonal cycle removed) of monthly mean zonal-mean zonal winds averaged over 55–65° S. The input data to the EOF were ordered from April to March each year for pressure-level data extending from 1,000 to 1 hPa. The returned first EOF eigenvector is a function of height (pressure level) and month of the year (April–March) (Fig. 1b). The first principal component time series (the S–T coupled mode index; Fig. 1a) consists of one value each year. The S–T coupled mode explains 42% of the total variance of the Antarctic circumpolar flow in the height–calendar month domain. For this calculation, we used the ERA-Interim reanalysis for the period April 1979–March 2017. The robustness of the S–T coupled mode is also confirmed by its reproducibility using the Japanese 55-year Reanalysis (JRA-55) data[46] (Supplementary Fig. 12).

We used 0.8σ of the S–T coupled mode index as a threshold to select significant vortex weakening years. We chose 0.8σ to include as many cases as possible that had a clear vortex weakening signal through the SH polar stratosphere to troposphere. The significant vortex weakening years were compared with all the other years (the index $< 0.8\sigma$), which included the years of insignificant vortex weakening events as well as those of neutral and vortex strengthening events. The comparison was done between significant vortex weakening events and all the other events because the impact of SH stratospheric vortex strengthening on Australian climate was much weaker than that of the vortex weakening and was not significantly different from the normal conditions at the 10% level, assessed by a permutation test (two-sided) with 4,000 times of resampling (Supplementary Fig. 13).

We monitored the tropospheric SAM using the monthly mean index values from the Climate Prediction Center (CPC) Antarctic Oscillation (AAO) index. This index is based on the leading EOF of monthly mean 700 hPa geopotential heights poleward of 20° S (ref. [5]) using the National Centers for Environmental Prediction (NCEP)/National Center for Atmospheric Research (NCAR) reanalysis data[47].

The McArthur FFDI is commonly used in Australia for climatological analysis of dangerous atmospheric conditions associated with wildfires. Daily values of FFDI are available from 1950 onward[32]. The FFDI data are based on the AWAP gridded analysis of daily maximum temperatures, vapour pressure at 15:00 LT (used together with temperature to calculate relative humidity near the time of maximum temperature) and daily accumulated precipitation totals for the 24-h period to 9:00 LT each day. The FFDI data are also based on wind speed at 6:00 UT representing mid-afternoon conditions over the longitude range spanned by Australia, which is from the NCEP/NCAR reanalysis[47] with bias correction applied to provide a better match to the wind speeds used for issuing forecasts of the FFDI by the Bureau of Meteorology. The set of weather and fuel moisture conditions that the FFDI represents are important risk factors for wildfire occurrence, as is the focus of this study, while noting additional factors that can influence fire occurrence such as a range of ignition sources (for example, lightning and human-caused sources) and fuel conditions (for example, fuel load and structure). Thus, the high impact of the vortex weakening on dangerous weather conditions for wildfires (as represented by the FFDI) may not necessarily lead to higher frequency of wildfire, which needs further investigation.

Removal of the influence of ENSO and long-term trends from the data. Dominant modes of sea surface temperature (SST) variability of the tropical Indo-Pacific, such as ENSO and the IOD, and a long-term linear trend are also important drivers of Australian climate variability and trend, respectively[7,8,48]. Lim et al.[18] reported that there was no significant correlation detected between ENSO indices and the S–T coupled mode index and no significant linear trend in the S–T coupled mode index over 1979–2016. Nonetheless, to detect the role of the polar vortex weakening on the Australian climate in a clean manner, we removed the influence of ENSO and the linear trends over 1979–2016 from the SAM index and all the variables analysed in the study: Australian T_{max}, T_{min}, rainfall and FFDI and MSLP, GPH500, ω500 and total cloud cover fields. For this calculation, we used a multiple linear regression model with three predictors—the Niño3 and El Niño Modoki indices[49], which monitor the eastern Pacific and central Pacific ENSO, respectively, and time—to capture the trend. As the IOD strongly covaries with Niño3 SSTs in the austral spring season[50], and generally decays during November in association with the onset of the Australian summer monsoon[4], we did not include the IOD as an additional predictor. The SST indices were derived using the merged SST dataset of ref. [51] for 1979–1981 and the Optimum Interpolation (OI) v2 SST dataset of ref. [52] for 1982–2017.

Statistical significance tests. In Figs. 2, 3 and 5, statistical significance was assessed using a resampling approach (permutation test) by randomly sampling without replacement 9 yr from the full record of 38 yr. Resampling was done 4,000 times. For the test on the difference between the two means (that is, the 9 vortex weakening years and the 29 vortex non-weakening years), the null hypothesis was that the difference is zero, and it was rejected if the observed difference was outside of the 95% and 90% confidence intervals for Figs. 2 and 5, respectively (by a two-tailed test). For the test on the ratio of the probability of occurrence of extreme events between the two groups, the null hypothesis was that the ratio is 1. The ratio of the probability of extreme events in the randomly picked 9 yr to the probability of those in the remaining 29 yr was formed 4,000 times and sorted. The null hypothesis was rejected if the ratio was greater than the top 2.5% threshold (that is, the high tail of the 95% confidence interval; a one-sided test).

Data availability

The datasets used in this study are available online in the following locations: ERA-Interim reanalysis, https://apps.ecmwf.int/datasets/data/interim-full-daily/levtype=sfc/; JRA-55 reanalysis, https://jra.kishou.go.jp/JRA-55/index_en.html; Hurrell et al. merged SST analysis, https://climatedataguide.ucar.edu/climate-data/merged-hadley-noaaoi-sea-surface-temperature-sea-ice-concentration-hurrell-et-al-2008; Reynolds OI v2 SST analysis, https://www.esrl.noaa.gov/psd/data/gridded/data.noaa.oisst.v2.html; AWAP analysis, http://www.bom.gov.au/climate/data-services/maps.shtml; CPC AAO index, https://www.cpc.ncep.noaa.gov/products/precip/CWlink/daily_ao_index/aao/aao.shtml. FFDI data are available by contacting the contributing author A.J.D. (andrew.dowdy@bom.gov.au). All the other data used for the analysis in this study are available by contacting the corresponding author.

Code availability

All the codes and scripts used for the analysis in this study are available by contacting the corresponding author.

References

44. Dee, D. et al. The ERA-Interim reanalysis: configuration and performance of the data assimilation system. *Q. J. R. Meteorol. Soc.* **137**, 553–597 (2011).
45. Jones, D., Wang, W. & Fawcett, R. High-quality spatial climate datasets for Australia. *Aust. Meteorol. Oceanogr. J.* **58**, 233–248 (2009).
46. Kobayashi, S. et al. The JRA-55 reanalysis: general specifications and basic characteristics. *J. Meteorol. Soc. Jpn Ser. II* **93**, 5–48 (2015).
47. Kalnay, E. et al. The NCEP/NCAR 40-year reanalysis project. *Bull. Am. Meteorol. Soc.* **77**, 437–471 (1996).
48. Jones, D. A. & Trewin, B. C. On the relationships between the El Niño–Southern Oscillation and Australian land surface temperature. *Int. J. Climatol.* **20**, 697–719 (2000).
49. Ashok, K., Behera, S. K., Rao, S. A., Weng, H. & Yamagata, T. El Niño Modoki and its possible teleconnection. *J. Geophys. Res. Oceans* **112**, C11007 (2007).
50. Lim, E.-P. et al. Dynamical forecast of inter–El Niño variations of tropical SST and Australian spring rainfall. *Mon. Weather Rev.* **137**, 3796–3810 (2009).
51. Hurrell, J. W., Hack, J. J., Shea, D., Caron, J. M. & Rosinski, J. A new sea surface temperature and sea ice boundary dataset for the community atmosphere model. *J. Clim.* **21**, 5145–5153 (2008).
52. Reynolds, R. W., Rayner, N. A., Smith, T. M., Stokes, D. C. & Wang, W. An improved in situ and satellite SST analysis for climate. *J. Clim.* **15**, 1609–1625 (2002).